Clean-NeRF: Reformulating NeRF to account for View-Dependent Observations

Xinhang Liu
HKUST

Yu-Wing Tai
HKUST

Chi-Keung Tang
HKUST

Abstract

While Neural Radiance Fields (NeRFs) had achieved unprecedented novel view synthesis results, they have been struggling in dealing with large-scale cluttered scenes with sparse input views and highly view-dependent appearances. Specifically, existing NeRF-based models tend to produce blurry rendering with the volumetric reconstruction often inaccurate, where a lot of reconstruction errors are observed in the form of foggy "floaters" hovering within the entire volume of an opaque 3D scene. Such inaccuracies impede NeRF's potential for accurate 3D NeRF registration, object detection, segmentation, etc., which possibly accounts for only limited significant research effort so far to directly address these important 3D fundamental computer vision problems to date. This paper analyzes the NeRF's struggles in such settings and proposes **Clean-NeRF** *for accurate 3D reconstruction and novel view rendering in complex scenes. Our key insights consist of enforcing effective appearance and geometry constraints, which are absent in the conventional NeRF reconstruction, by 1) automatically detecting and modeling view-dependent appearances in the training views to prevent them from interfering with density estimation, which is complete with 2) a geometric correction procedure performed on each traced ray during inference. Clean-NeRF can be implemented as a plug-in that can immediately benefit existing NeRF-based methods without additional input. Codes will be released.*[1]

1. Introduction

Neural Radiance Fields (NeRFs) [37] have made revolutionary contributions in novel view synthesis [2, 3], autonomous driving [47, 55], digital human [19, 72], and 3D content generation [10, 44, 32]. To date, unfortunately, most NeRF-based methods encounter challenges when tackling large-scale cluttered scenes (e.g., Fig. 1):

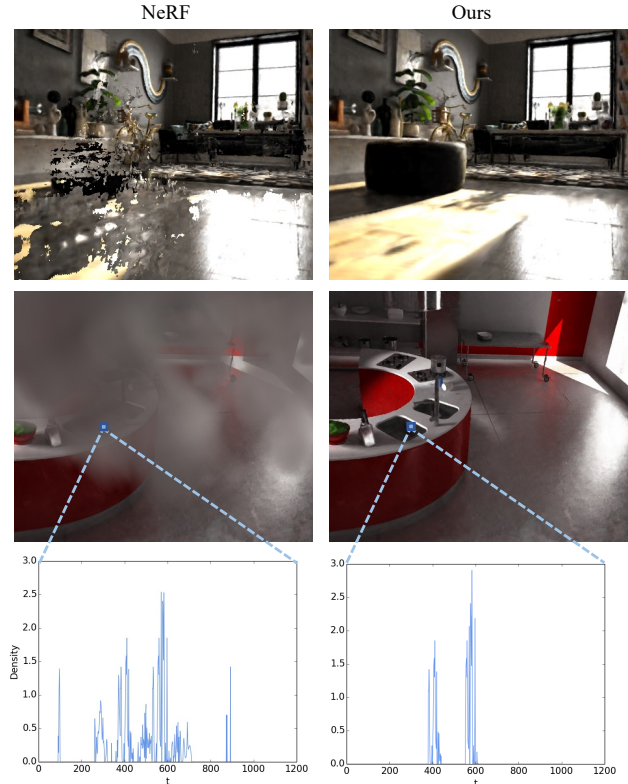1. Input observations used for NeRF are often too sparse compared to forward-facing or synthetic looking-inward

---

Figure 1. *Foggy* vs *Clear* **NeRF.** Our Clean-NeRF gets rid of reconstruction errors manifested as foggy "floaters" in the density volume without additional input or significant computational overhead. Below are density profiles along a given ray before and after our geometry correction procedure, where we discard density peaks corresponding to floaters.

scenes;

2. View-dependent visual effects give rise to ambiguity, resulting in a "foggy" density field as shown in Fig. 1. Such artifacts are particularly pronounced in indoor scenes strewn with view-dependent appearances, such as specular highlights, glossy surface reflections from man-made objects.

Despite attempts to enhance NeRF's rendering quality given suboptimal input, such as using 3D conical frustums [2, 3], physically-grounded augmentations [12], and

misalignment correction [23], these challenges have yet to be fully resolved. Depth supervision [13, 63] or proxy geometry [65, 64] images can help alleviate the challenges in handling large-scale with sparse input, at the expense of expensive pre-processing or additional input. Another line of work [61, 42, 59] achieves better reconstruction of surface geometry by using signed distances instead of volume density as scene representation. However, they sacrifice the ability to synthesize photo-realistic novel views.

To address the above issues, we propose an extension to NeRF, dubbed as **Clean-NeRF**, which enforces effective *appearance* and *geometry* constraints conducive to accurate colors and 3D densities estimation. We believe Clean-NeRF can contribute beyond novel view synthesis, such as NeRF object detection [21], NeRF object segmentation [73, 34, 16, 48], and NeRF registration [18], where the rooms for improvement are substantial if more accurate color and density estimation are available.

Correspondingly, there are two steps in Clean-NeRF. First, for appearance correction, the view-independent and view-dependent color components are predicted from the underlying 3D scene, which is combined to produce the final color estimation (Fig. 2). The view-independent component (diffuse color and shading) captures the overall scene color, while the view-dependent component (highlights or reflections) captures color variations due to changes in viewing angle. Clean-NeRF then discards these view-dependent appearances in the training views to prevent them from interfering with the density estimation. Second, a simple and effective geometry correction procedure will be performed to further eliminate the foggy "floaters" or density errors. This geometry correction procedure is based on an assumption in line with traditional ray tracing in computer graphics. Experiments verify that our proposed Clean-NeRF can effectively get rid of floater artifacts without additional input.

In summary, our contributions include the following:

- We propose a concise method for decomposing view-independent and view-dependent appearance during NeRF training and eliminate the interference of view-dependent appearance.
- We propose a geometric correction procedure performed on each traced ray during inference to refine the density estimation and better tackle the floater artifacts.
- Extensive experiments and ablations verify the effectiveness of our core designs and results in improvements over the vanilla NeRF and other state-of-the-art alternatives.

2. Related Works

Neural Radiance Fields. NeRFs debut in [37] achieved unprecedented novel view synthesis effects, by modeling the underlying 3D scene as a continuous volumetric field of
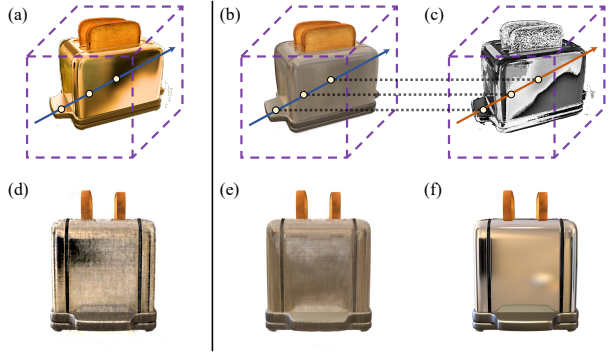

Figure 2. **Appearance Decomposition. (a, d)** For object surfaces with strong view-dependent effects, vanilla NeRF often gets disrupted, resulting in poor reconstruction quality. We propose decomposing appearance into **(b)** view-independent and **(c)** view-dependent components during NeRF training and incorporating geometry-related priors to improve reconstruction quality. Our approach shows the ability to **(e)** render the view-independent component of the scene and **(f)** more accurate recovery of the scene.

color and density via layers of MLP. The input to a NeRF consists of a 5D vector containing a 3D location (x, y, z), and a 2D viewing direction (θ, ϕ). Since then, follow-up works have addressed the limitations and improved the performance, such as enabling dynamic modeling [69, 43, 45, 56], efficient inference [67, 17, 11, 35, 38, 60], editing [33, 69, 58, 22, 25], and multi-task learning [73, 34, 16].

Much effort has been made to improve the accuracy of NeRF's rendered novel views and reconstructed geometry. Mip-NeRF [2] mitigates unsightly aliasing artifacts in NeRF in representing coarse and fine details. Mip-NeRF 360 [3] uses a non-linear scene parameterization and online distillation to tackle unbounded scenes. Aug-NeRF [12] leverages worst-case perturbations to enable NeRF in smoothness-aware geometry reconstruction. Reg-NeRF [41] renders patches from unobserved viewpoints for a given radiance field and regularizes appearance and geometry. AligNeRF [23] addresses misalignment problems caused by moving objects or small camera calibration errors. DS-NeRF [13] takes advantage of readily-available depth supervision from SfM. NerfingMVS [63] employs adapted depth priors from a monocular depth network to guide the sampling process of volume rendering.

Reflectance Decomposition. To acquire reflectance data, sophisticated devices have traditionally been necessary to sample the light-view space [24, 36, 40]. Subsequent research has proposed practical techniques for acquiring spatially varying BRDFs, such as those presented in [24, 36, 40, 39]. More recently, deep learning methods have made it possible to acquire BRDF information from a single flash image [31, 30, 14].

In the context of NeRF, highly reflective objects can pose challenges in the reconstruction and relighting pro-

cess. Previous works have attempted to address this issue by decomposing appearance into scene lighting and materials, but these methods assume known lighting [7, 54] or no self-occlusion [8, 9, 70]. Ref-NeRF [57] uses a representation of reflected radiance and structures this function using a collection of spatially-varying scene properties to reproduce the appearance of glossy surfaces. Despite these advances, Ref-NeRF requires accurate normal vectors and outgoing radiance estimation, which is difficult to obtain for sparse input views. In addition, effectively addressing the view-dependent appearance problem in the context of large scenes and sparse observations remains a challenge. To address this issue, we propose a simple yet effective decomposition method to eliminate its interference without the need to estimate surface normals or outgoing radiance.

Intrinsic Image Decomposition. Barrow and Tenenbaum introduced intrinsic images as a valuable intermediate representation for scenes [4], assuming that an image can be expressed as the pointwise product of the object's true colors or reflectance and the shading on that object. This can be represented as $I = R \cdot S$, where I, R, and S denote the image, the reflectance, and the shading, respectively.

Early optimization-based works addressed the problem of separating an image into its reflectance and illumination components by assuming that large image gradients correspond to reflectance changes and small gradients to lighting changes [26, 20]. Incorporation of additional priors improves the accuracy and robustness, such as reflectance sparsity [50, 52], low-rank reflectance [1] and distribution difference in gradient domain [6, 27]. Deep learning methods [15, 68, 74, 28, 29] have emerged to perform intrinsic image decomposition, estimating the reflectance and shading on labeled training data. Notably and differently, in intrinsic image decomposition, where shadows and highlights are separated as high-frequency components, these components *may* still be separated as view-independent in our Clean-NeRF as long as they are *consistent* across all input views, e.g., a static shadow is consistently observed across all views. Thus, intrinsic image decomposition is inappropriate (both overkill and inadequate) to the "vi-vd" decomposition of Clean-NeRF.

IntrinsicNeRF [66] introduces intrinsic decomposition to the NeRF-based neural rendering method, which allows for editable novel view synthesis in room-scale scenes. Compared with our simple and effective appearance decomposition, IntrinsicNeRF requires dense inputs (900 images for their indoor Replica scene), which assumes the NeRF reconstruction is accurate.

3. Method

In this section, we present Clean-NeRF to effectively address the floater artifacts caused by current inaccurate NeRF
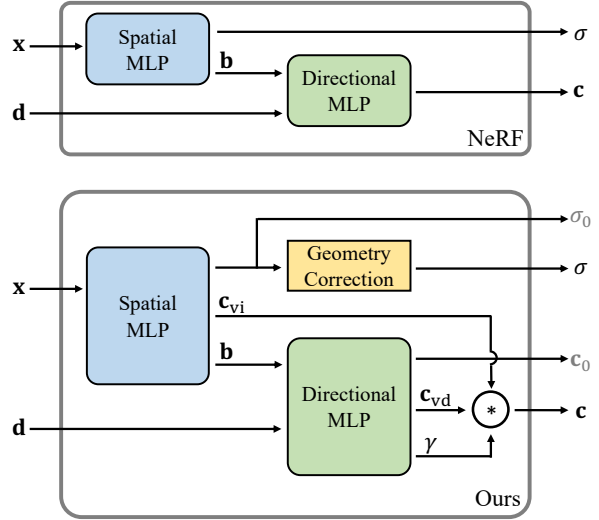

Figure 3. **Vanilla NeRF and Clean-NeRF architectures.** Similar to vanilla NeRF, we estimate density σ_0 and color $\mathbf{c}_0$ from the spatial MLP and the directional MLP. On the other hand, we propose "vi-vd" appearance decomposition based on spherical harmonics (SHs) and obtain a final color estimation $\mathbf{c}$ by summing the view-independent color component $\mathbf{c}_{vi}$ produced by the spatial MLP, with the view-dependent color component $\mathbf{c}_{vd}$ produced by the directional MLP. Then a geometry correction procedure refines the initial estimation and obtains the final density estimation σ.

reconstruction. Clean-NeRF can be applied as an easy plug-in component into any existing NeRF-like models, including MLP-based and voxel grid-based approaches, without resorting to extra knowledge such as normal maps, depth maps, or lighting conditions. In Sec. 3.1, we introduce the overall architecture of Clean-NeRF compared to the vanilla NeRF. Sec. 3.2 describes our principled implementation for decomposing an appearance into view-dependent ("vd") and view-independent ("vi") components to achieve better novel view synthesis and 3D geometry reconstruction. Finally, we present our geometry correction strategy in Sec. 3.3.

3.1. Overall Architecture

Fig. 3 compares vanilla NeRF [37] and our model, both taking a sampled spatial coordinate point $\mathbf{x} = (x, y, z)$ and direction $\mathbf{d} = (\theta, \phi)$ as input and output the volume density and color.

Vanilla NeRF uses a spatial MLP to estimate volume density σ at position $\mathbf{x}$. Then the directional MLP takes as input the direction $\mathbf{d}$ as well as spatial feature $\mathbf{b}$ to estimate a view-depenent output color $\mathbf{c}$. In Clean-NeRF architecture, we also use the spatial MLP and the directional MLP to output an initial estimation of density σ_0 and color $\mathbf{c}_0$, similar to the vanilla NeRF. The initial estimation of color corresponding to ray $\mathbf{r}(t) = \mathbf{o} + t\mathbf{d}$ can be evaluated from

σ_0 and $\mathbf{c}_0$:

$$\hat{\mathbf{C}}_0 = \sum_{k=1}^{K} \hat{T}_0(t_k)\alpha(\sigma_0(t_k)\delta_k)\mathbf{c}_0(t_k), \qquad (1)$$

where $\hat{T}_0(t_k) = \exp\left(-\sum_{k'=1}^{k-1} \sigma_0(t_k)\delta(t_k)\right)$, $\alpha(x) = 1 - \exp(-x)$, and $\delta_p = t_{k+1} - t_k$. Without requiring additional inputs, Clean-NeRF differs from vanilla NeRF in that while making the initial estimation, we also predict the view-independent color component $\mathbf{c}_{\text{vi}}$ with the spatial MLP and the view-dependent color component $\mathbf{c}_{\text{vd}}$ with the directional MLP. We supervise these estimations by performing an SH-based decomposition of the initial color estimation $\mathbf{c}_0$, as described in Sec. 3.2. The directional MLP also estimates a view-dependent factor γ and we obtain a final color estimation $\mathbf{c}$ by:

$$\mathbf{c} = \gamma\mathbf{c}_{\text{vi}} + (1 - \gamma)\mathbf{c}_{\text{vd}}. \qquad (2)$$

Note that $\mathbf{c}_{\text{vi}}$ captures the overall scene color while $\mathbf{c}_{\text{vd}}$ captures the color variations due to changes in viewing angle. By blending these two components with the factor γ, we can synthesize a faithful color of the underlying 3D scene, even from a limited number of input views.

To better eliminate the floating artifacts, we propose a geometry correction procedure on σ_0 to correct the initial density estimation and obtain the final density estimation σ, as described in Sec. 3.3. Such procedure is based on practical assumptions and is easy to implement.

The final estimation of color corresponding to ray $\mathbf{r}(t) = \mathbf{o} + t\mathbf{d}$ is then computed as

$$\hat{\mathbf{C}} = \sum_{k=1}^{K} \hat{T}(t_k)\alpha(\sigma(t_k)\delta_k)\mathbf{c}(t_k), \qquad (3)$$

where $\hat{T}(t_k) = \exp\left(-\sum_{k'=1}^{k-1} \sigma(t_k)\delta(t_k)\right)$, $\alpha(x) = 1 - \exp(-x)$, and $\delta_p = t_{k+1} - t_k$. We train the network using photometric loss based on both the initial and the final estimations

$$\mathcal{L}_{\text{pho}} = \sum_{\mathbf{r} \in \mathcal{R}} \left\| \hat{\mathbf{C}}_0(\mathbf{r}) - \mathbf{C}(\mathbf{r}) \right\|_2^2 + \left\| \hat{\mathbf{C}}(\mathbf{r}) - \mathbf{C}(\mathbf{r}) \right\|_2^2. \qquad (4)$$

3.2. Appearance Decomposition

To guide our vi-vd decomposition, we utilize Spherical harmonics (SHs) which are widely used as a low-dimensional representation for spherical functions, and have been used to model Lambertian surfaces [46, 5] as well as glossy surfaces [53]. To use SH functions to model a given function, we query the SH functions $Y_\ell^m : \mathbb{S}^2 \mapsto \mathbb{R}$ at a viewing angle $\mathbf{d}$ and then fit the estimation $\mathbf{c}_0$ by finding the corresponding coefficients. We use low-degree

SH functions to compute ideal values of view-independent color components, and high-degree SH functions for view-dependent components. In this subsection, we will perform all of our calculations at an arbitrary position $\mathbf{x}$ in space, and therefore we will omit the symbol $\mathbf{x}$ from our notation.

We use $\mathbf{y}(\mathbf{d}) \in \mathbb{R}^L$ to represent the set of SH function values at the viewing angle $\mathbf{d}$:

$$\mathbf{y}(\mathbf{d}) = \left[Y_0^0(\mathbf{d}), Y_1^{-1}(\mathbf{d}), Y_1^0(\mathbf{d}), Y_1^1(\mathbf{d}), \dots, Y_{\ell_{\max}}^{\ell_{\max}}(\mathbf{d}) \right]^\top, \qquad (5)$$

where $L = (\ell_{\max} + 1)^2$. To ensure clarity, we will use $c : \mathbb{S}^2 \mapsto \mathbb{R}$ to represent one of the three channels of $\mathbf{c}_0$ at a given position $\mathbf{x}$ (also c_{vi} and c_{vd}), noting the derivation should be readily extended to all three channels. We begin by sampling a set of N viewing angles $\mathbf{d_i}, 1 \leq i \leq N \subset \mathbb{S}^2$. The colors of all the sample directions are represented using a vector $\mathbf{s} \in \mathbb{R}^N$:

$$\mathbf{s} = \begin{bmatrix} c(\mathbf{d}_1) & c(\mathbf{d}_2) & \dots & c(\mathbf{d}_{N-1}) & c(\mathbf{d}_N) \end{bmatrix}^\top \qquad (6)$$

The coefficients to be determined are represented by a vector $\mathbf{k} \in \mathbb{R}^L$. To find the optimal coefficients that fit the view-dependent color estimation, we solve the following optimization problem:

$$\min_{\mathbf{k} \in \mathbb{R}^L} \|\mathbf{s} - \mathbf{Y}\mathbf{k}\|_2^2, \qquad (7)$$

where

$$\mathbf{Y} = \begin{bmatrix} \mathbf{y}(\mathbf{d}_1) & \mathbf{y}(\mathbf{d}_2) & \dots & \mathbf{y}(\mathbf{d}_{N-1}) & \mathbf{y}(\mathbf{d}_N) \end{bmatrix}. \qquad (8)$$

This is a standard linear regression problem, where we seek to find the values of the coefficient vector $\mathbf{k}$ which minimizes the least squares error between the vector $\mathbf{s}$ and the linear combination of the columns of $\mathbf{Y}$, weighted by the coefficients in $\mathbf{k}$. Using the normal equation, the solution is given by:

$$\mathbf{k}^* = (\mathbf{Y}^\top \mathbf{Y})^{-1} \mathbf{Y}^\top \mathbf{s} \qquad (9)$$

We can use the solution coefficients $\mathbf{k}^*$ as weights to linearly combine SH functions. Retaining the low-degree SH functions allows us to capture the view-independent appearance of the scene. Conversely, including high-degree SH functions leads to a high-frequency view-dependent residue. To differentiate between the two, we denote the low-degree and high-degree functions as L_{low} and L_{high}, respectively. To compute ideal values for the view-independent component, we can use the solution coefficients and apply the following equation:

$$\tilde{c}_{\text{vi}} = \sum_{i=1}^{L_{\text{low}}} \frac{1}{4\pi r^2} \iint_{\mathbb{S}^2} k_i^* y_i(\mathbf{d}) \sin\theta d\theta d\phi, \qquad (10)$$

where we take the mean value around the $\mathbb{S}^2$ surface. In our implementation, we approximate it by

$$\tilde{c}_{\text{vi}} = \sum_{i=1}^{L_{\text{low}}} \sum_{i=1}^{N} k_i^* y_i(\mathbf{d_i}), \qquad (11)$$
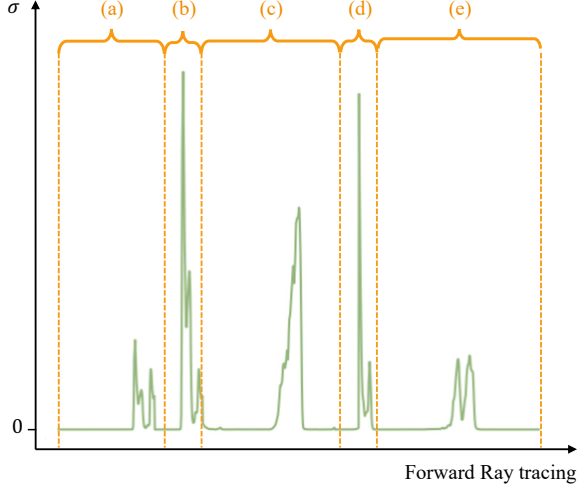
Figure 4. **An example traced ray's density profile.** Peaks in region (a) and region (e) appear as floating artifacts and would interfere with the rendering process.

This value is then used to guide the output of the view-independent color component $\mathbf{c}_{\text{vi}}$ from the spatial MLP using a regularizer. Specifically, we use the following equation to compute the vi-regularizer loss $\mathcal{L}_{\text{vi}}$:

$$\mathcal{L}_{\text{vi}} = (\mathbf{c}_{\text{vi}} - \tilde{\mathbf{c}}_{\text{vi}})^2. \qquad (12)$$

We apply the following equation to compute optimal values for the view-dependent component:

$$\tilde{c}_{\text{vd}}(\mathbf{d}) = \sum_{i=L_{\text{high}}}^{L} k_i^* y_i(\mathbf{d}). \qquad (13)$$

Incorporating the computed value to guide the output of the view-dependent color residue $\mathbf{c}_{\text{vd}}$ from the directional MLP using the vd-regularizer loss:

$$\mathcal{L}_{\text{vd}} = \left\| \begin{bmatrix} \mathbf{c}_{\text{vd}}(\mathbf{d_1}) \\ \vdots \\ \mathbf{c}_{\text{vd}}(\mathbf{d_N}) \end{bmatrix} - \begin{bmatrix} \tilde{\mathbf{c}}_{\text{vd}}(\mathbf{d_1}) \\ \vdots \\ \tilde{\mathbf{c}}_{\text{vd}}(\mathbf{d_N}) \end{bmatrix} \right\|_2^2. \qquad (14)$$

As aforementioned we consider a given position $\mathbf{x}$ in the space, while in actual implementation we take the ℓ_2-norm among all the positions in a sampled batch for Eqn. 12 and Eqn. 14.

3.3. Geometry Correction

Clean-NeRF is consistent with standard NeRF in that an initial density estimation, denoted as σ_0, is generated for volume rendering with the initial color estimation $\mathbf{c}_0$. We propose a geometry correction strategy for the final rendering that simultaneously refine the density estimation while better handling unsightly floater artifacts.

To understand our working principle, without losing generality, consider a given ray intersecting an opaque 3D scene

consisting of a single sphere. In the absence of noise, there exist at most two relevant intersections, corresponding to the front and back surface visible from the camera at both ray directions. This is in line with traditional ray tracing in computer graphics, where only the ray-object intersection closest to the camera should be returned. Figure 4 shows a density profile along a given ray, where the two salient peaks respectively correspond to the closest front and back surface visible along the ray in both camera view directions. Other peaks along the same ray will either manifest as foggy floaters hovering in the density volume or correspond to surfaces in the scene that are hidden by the front and back surfaces and, thus should not be visible or rendered at all.

Thus, our geometry correction strategy given by Alg. 1 begins the density decomposition process by performing a forward ray tracing to identify the first salient peak $k_{\text{peak}}^{\text{front}}$ from the front-facing direction, followed by a backward ray tracing pass to identify the first salient peak $k_{\text{peak}}^{\text{back}}$ from the back-facing direction. We then retain the density component within and between the neighborhoods of $k_{\text{peak}}^{\text{front}}$ and $k_{\text{peak}}^{\text{back}}$ and zero the rest[2].

Algorithm 1 Geometry Correction

Input: $\{\sigma_0(t_k)\}_{k=1,\dots,K}, \sigma_{\text{thres}}, m$
Output: $\{\sigma(t_k)\}_{k=1,\dots,K}$
1: **for** $k \leftarrow 1$ to K **do**   // Forward pass ray tracing.
2:      **if** $\sigma_0(t_k) > \sigma_{\text{thres}}$ **then**
3:          $k_{\text{peak}}^{\text{front}} \leftarrow k$
4:          **break**
5: **for** $k \leftarrow K$ to 1 **do**   // Backward pass ray tracing.
6:      **if** $\sigma_0(t_k) > \sigma_{\text{thres}}$ **then**
7:          $k_{\text{peak}}^{\text{back}} \leftarrow k$
8:          **break**
9: **for** $k \leftarrow 1$ to K **do**
10:      **if** $k < k_{\text{peak}}^{\text{front}} - m$ **or** $k > k_{\text{peak}}^{\text{back}} + m$ **then**
11:          $\sigma(t_k) \leftarrow 0$
12:      **else**
13:          $\sigma(t_k) \leftarrow \sigma_0(t_k)$
     return $\{\sigma(t_k)\}_{k=1,\dots,K}$

Refer to Fig. 4 again: peaks in region (a) and region (e) appear as floating artifacts and would interfere with the rendering process, and so they are discarded. Notably, multiple salient peaks may exist corresponding to other surface points along the ray, such as region (d), e.g., corresponding to the two slices of toast intersected by the pertinent ray in the previous figure. If the salient peak (d) is further from the ray origin but lower than (b), as Fig. 4 shows, the corresponding surface point is occluded by (b), which can be safely detected by backward pass while occlusion-correct

---

[2]With abuse of language, salient plateaus are also referred to as "peaks", which are also detected using Alg. 1 if the pertinent ray hits a solid (sphere).

| Ground Truth | View-independent Component | Color | Ground Truth | View-independent Component | Color |

Figure 5. **Qualitative evaluation of Clean-NeRF on Shiny Blender dataset.** We render the view-independent component image, and the final color image combining both view-independent and view-dependent components to compare with the ground truth.
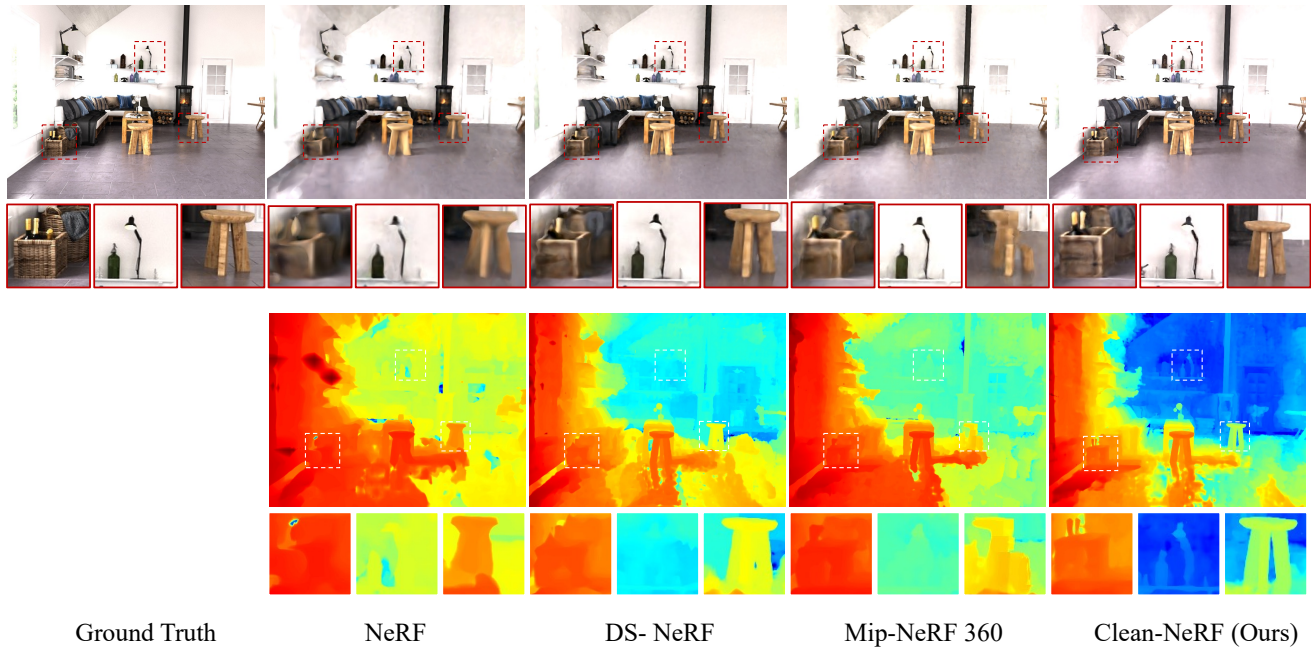

| Ground Truth | NeRF | DS- NeRF | Mip-NeRF 360 | Clean-NeRF (Ours) |

Figure 6. **Qualitative Comparison between Clean-NeRF and baselines.** Clean-NeRF recovers intricate object details while removing annoying "floaters" even when observations are sparse.

rendering is unaffected, as peak (d) is lower. Otherwise, suppose the peak (d) is higher (e.g., the toast further back is higher), then the peak in (b) should have been clamped to reveal the true geometry (d) as the first salient peak as seen from the ray origin.

4. Results

In this section, we provide comparisons with previous state-of-the-art NeRF-based methods and evaluation of our main technical components, both qualitatively and quan-

titatively. We first evaluate our proposed Clean-NeRF on Shiny Blender dataset [57] containing different glossy objects rendered in Blender under conditions similar to typical NeRF's datasets, to verify our model's ability to handle challenging material properties by proper decomposition of observed appearance into the corresponding view-independent and view-dependent components. We then run our proposed Clean-NeRF on Hypersim dataset [49], a challenging synthetic dataset of photo-realistic indoor scenes. We use the given accurate camera poses for Shiny Blender and use colmap [51] to estimate camera poses for Hypersim.

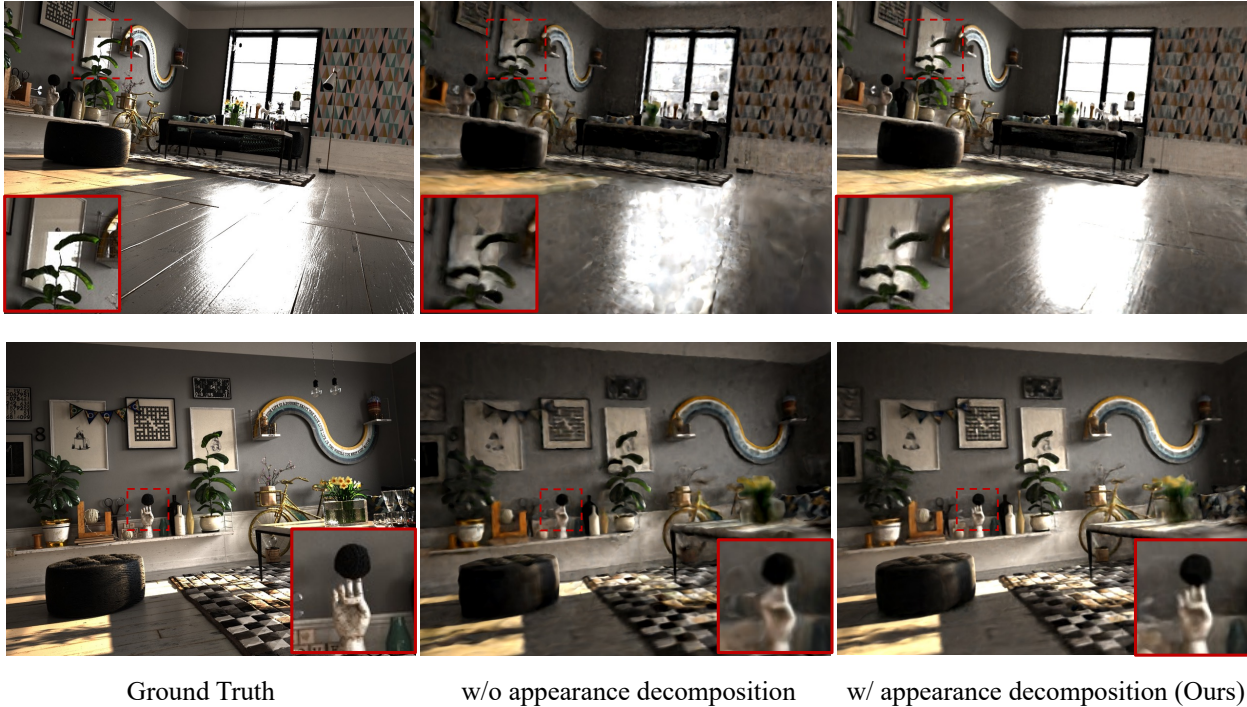| Ground Truth | w/o appearance decomposition | w/ appearance decomposition (Ours) |

Figure 7. **Qualitative evaluation on appearance decomposition.** Without appearance decomposition, our model fails to recover the glossy objects such as the glass, the floor, and the plant.

We train our Clean-NeRF for 500K iterations to guarantee convergence on a single NVIDIA GeForce RTX 3090 Ti GPU. For Shiny Blender, we use 100 input views for training. For Hypersim, we use around 50 to 80 input views for training, depending on the scale of the scene. All the shown cases and reported metrics are from held-out views. We report three error metrics, including peak signal-to-noise ratio (PSNR), structural similarity index measure (SSIM) [62], mean absolute error (MAE), and learned perceptual image patch similarity (LPIPS) [71]. We include more experiment details and results in the supplemental material, including videos, and encourage the readers to check them.

Appearance Decomposition on Glossy Objects   To verify Clean-NeRF's ability to decompose object appearances into the corresponding view-independent and view-dependent components, we evaluate Clean-NeRF on Shiny Blender dataset and render the view-independent component image and color image with both view-independent and view-dependent components (Fig. 5).

Comparison on Challenging Indoor Scenes   We compare Clean-NeRF with NeRF [37], mip-NeRF 360 [3] and DS-NeRF [13], which are representative NeRF-based methods and strong baselines for large-scale scenes. As shown in Fig. 6 and Tab 1, our method recovers intricate details of objects in the indoor scene, especially objects with glossy surfaces, and has few observations. Note that DS-NeRF

uses sparse depth maps for supervision, while our method and other baselines do not.

Ablation Study on our Architecture Design   We qualitatively and quantitatively evaluate the main components of Clean-NeRF.

Fig. 7 shows that without appearance decomposition, NeRF struggles to recover the glossy floor and plants. Fig. 8 shows that without geometry correction, the NeRF needs to generate floaters in order to explain the view-dependent observations. Quantitative evaluations are given in Tab. 1.

	best	second-best		
Method	PSNR↑	SSIM↑	MAE↓	LPIPS↓
NeRF	20.90	0.84	0.052	0.2509
Mip-NeRF 360	21.32	0.82	0.048	0.3399
DS-NeRF	26.27	0.89	0.03	0.2275
w/o app. dec.	22.93	0.85	0.041	0.21
w/o dec. geo.	25.88	0.86	0.0059	0.2299
Ours	27.29	0.89	0.041	0.1975

Table 1. **Quantitative comparison and evaluation.** We compare our proposed Clean-NeRF with representative NeRF-based methods and their variants.

5. Discussion and Limitations

Our method assumes fixed lighting condition and no semi-transparent objects in a scene. In addition, we observe

Ground Truth   w/o geometry correction   w/ geometry correction (Ours)
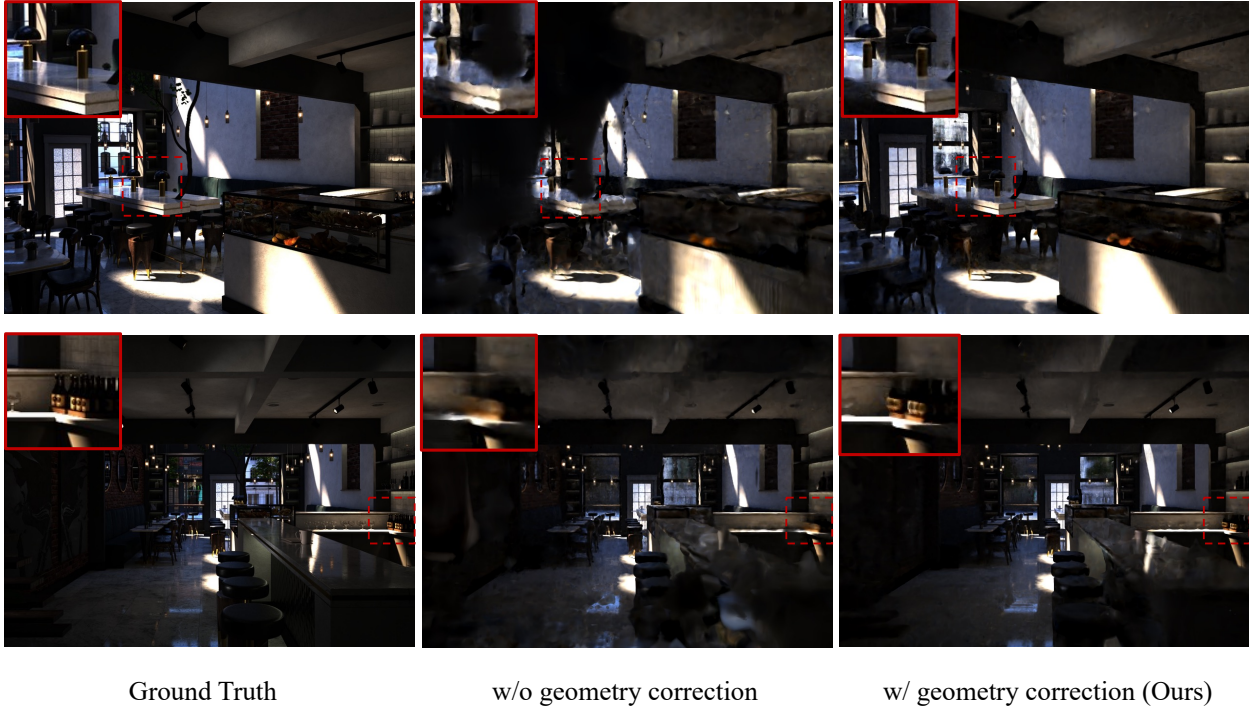
Figure 8. **Qualitative evaluation on geometry correction.** Without geometry correction NeRF tends to generate floaters.

that, when we deal with sparse inputs and the specular highlights of a point appear in most of the inputs, such highlights may be regarded as view-independent colors, since our method does not make any assumption about the surface properties and colors. Below, we discuss some important questions related to our work:

Why are there floaters in sparse but not in dense inputs? In vanilla NeRF, observation errors are backpropagated according to Eqn. 1, which are backpropagated equally to density and color along a given ray without any prior. With dense inputs, the strong geometry constraint from other view points can correct the density errors along a ray, and thus the view dependent observations will be correctly backpropagated to the color component. In contrast, when the number of inputs is limited, the network cannot resolve the ambiguity that the view dependent observations are caused by change of colors, or by the semi-transparent occluders, i.e., floaters. Since errors are backpropagated equally to both density and color along a ray, generating *floaters* is more preferable by Eqn. 1.

What are the benefits of vi- and vd- color decomposition? Such decomposition can stabilize the solution by reducing the ambiguity in handling view-dependent observations as residual errors in c_{vd}, while keeping the c_{vi} stable across multiple views, thus leading to a reconstruction of higher quality. Additionally, in downstream tasks such as NeRF object detection [21] and segmentation [48], one may have

to estimate the color of voxel features that is independent of viewpoints. Our c_{vi} can provide such voxel feature extraction for free without additional computations.

Why is the decomposition in Eqn. 2 correct? Eqn. 2 can be considered as a simplified BRDF model, e.g., a simplified Phong model with diffuse and specular components but without normal and light. Although not entirely physically correct, this formulation can handle most view-dependent observations in the real world without resorting to estimating surface normals and incoming lighting conditions, thus providing a fast and easy way to optimize. According to our experiments, this formulation is generally applicable, and the resulting decomposition is reasonably accurate.

6. Conclusion

This paper proposes *Clean-NeRF* for accurate 3D reconstruction and novel view rendering in complex scenes. By 1) detecting and discarding view-dependent appearances in training, followed by 2) a geometric correction procedure performed on each traced ray during inference, Clean-NeRF achieves unprecedented clarity and accuracy, capable of recovering intricate object details while rejecting "floaters" when only sparse observations are given. Codes will be released.

References

[1] Bousseau Adrien, Paris Sylvain, and Durand Frédo. User-assisted intrinsic images. *ACM Transactions on Graphics (TOG)*, 2009. 3

[2] Jonathan T Barron, Ben Mildenhall, Matthew Tancik, Peter Hedman, Ricardo Martin-Brualla, and Pratul P Srinivasan. Mip-nerf: A multiscale representation for anti-aliasing neural radiance fields. In *IEEE/CVF Conference on Computer Vision and Pattern Recognition (CVPR)*, pages 5855–5864, 2021. 1, 2

[3] Jonathan T Barron, Ben Mildenhall, Dor Verbin, Pratul P Srinivasan, and Peter Hedman. Mip-nerf 360: Unbounded anti-aliased neural radiance fields. In *IEEE/CVF Conference on Computer Vision and Pattern Recognition (CVPR)*, pages 5470–5479, 2022. 1, 2, 7

[4] Harry Barrow, J Tenenbaum, A Hanson, and E Riseman. Recovering intrinsic scene characteristics. *Computer Vision Systems*, 2(3-26):2, 1978. 3

[5] Ronen Basri and David W Jacobs. Lambertian reflectance and linear subspaces. *IEEE Transactions on Pattern Analysis and Machine Intelligence (PAMI)*, 25(2):218–233, 2003. 4

[6] Sai Bi, Xiaoguang Han, and Yizhou Yu. An l1 image transform for edge-preserving smoothing and scene-level intrinsic decomposition. *ACM Transactions on Graphics (TOG)*, 2015. 3

[7] Sai Bi, Zexiang Xu, Pratul Srinivasan, Ben Mildenhall, Kalyan Sunkavalli, Miloš Hašan, Yannick Hold-Geoffroy, David Kriegman, and Ravi Ramamoorthi. Neural reflectance fields for appearance acquisition. *arXiv preprint arXiv:2008.03824*, 2020. 3

[8] Mark Boss, Raphael Braun, Varun Jampani, Jonathan T Barron, Ce Liu, and Hendrik Lensch. Nerd: Neural reflectance decomposition from image collections. In *IEEE/CVF Conference on Computer Vision and Pattern Recognition (CVPR)*, pages 12684–12694, 2021. 3

[9] Mark Boss, Varun Jampani, Raphael Braun, Ce Liu, Jonathan Barron, and Hendrik Lensch. Neural-pil: Neural pre-integrated lighting for reflectance decomposition. *Advances in Neural Information Processing Systems (NeurIPS)*, 34:10691–10704, 2021. 3

[10] Eric R. Chan, Connor Z. Lin, Matthew A. Chan, Koki Nagano, Boxiao Pan, Shalini De Mello, Orazio Gallo, Leonidas J. Guibas, Jonathan Tremblay, Sameh Khamis, Tero Karras, and Gordon Wetzstein. Efficient geometry-aware 3d generative adversarial networks. In *IEEE/CVF Conference on Computer Vision and Pattern Recognition (CVPR)*, pages 16123–16133, June 2022. 1

[11] Anpei Chen, Zexiang Xu, Andreas Geiger, Jingyi Yu, and Hao Su. Tensorf: Tensorial radiance fields. In *European Conference on Computer Vision (ECCV)*, 2022. 2

[12] Tianlong Chen, Peihao Wang, Zhiwen Fan, and Zhangyang Wang. Aug-nerf: Training stronger neural radiance fields with triple-level physically-grounded augmentations. In *IEEE/CVF Conference on Computer Vision and Pattern Recognition (CVPR)*, pages 15191–15202, 2022. 1, 2

[13] Kangle Deng, Andrew Liu, Jun-Yan Zhu, and Deva Ramanan. Depth-supervised nerf: Fewer views and faster training for free. In *IEEE/CVF Conference on Computer Vision and Pattern Recognition (CVPR)*, pages 12882–12891, 2022. 2, 7

[14] Valentin Deschaintre, Miika Aittala, Fredo Durand, George Drettakis, and Adrien Bousseau. Single-image svbrdf capture with a rendering-aware deep network. *ACM Transactions on Graphics (TOG)*, 37(4):1–15, 2018. 2

[15] Qingnan Fan, Jiaolong Yang, Gang Hua, Baoquan Chen, and David Wipf. Revisiting deep intrinsic image decompositions. In *IEEE/CVF Conference on Computer Vision and Pattern Recognition (CVPR)*, pages 8944–8952, 2018. 3

[16] Zhiwen Fan, Peihao Wang, Yifan Jiang, Xinyu Gong, Dejia Xu, and Zhangyang Wang. Nerf-sos: Any-view self-supervised object segmentation on complex scenes. *International Conference on Learning Representations (ICLR)*, 2023. 2

[17] Sara Fridovich-Keil, Alex Yu, Matthew Tancik, Qinhong Chen, Benjamin Recht, and Angjoo Kanazawa. Plenoxels: Radiance fields without neural networks. In *IEEE/CVF International Conference on Computer Vision (ICCV)*, pages 5501–5510, 2022. 2

[18] Lily Goli, Daniel Rebain, Sara Sabour, Animesh Garg, and Andrea Tagliasacchi. nerf2nerf: Pairwise registration of neural radiance fields. *arXiv preprint arXiv:2211.01600*, 2022. 2

[19] Yang Hong, Bo Peng, Haiyao Xiao, Ligang Liu, and Juyong Zhang. Headnerf: A real-time nerf-based parametric head model. In *IEEE/CVF Conference on Computer Vision and Pattern Recognition (CVPR)*, pages 20374–20384, 2022. 1

[20] Berthold KP Horn. Determining lightness from an image. *Computer Graphics and Image Processing*, 3:277–299, 1974. 3

[21] Benran Hu, Junkai Huang, Yichen Liu, Yu-Wing Tai, and Chi-Keung Tang. Nerf-rpn: A general framework for object detection in nerfs. *IEEE/CVF Conference on Computer Vision and Pattern Recognition (CVPR)*, 2023. 2, 8

[22] Wonbong Jang and Lourdes Agapito. Codenerf: Disentangled neural radiance fields for object categories. In *IEEE/CVF International Conference on Computer Vision (ICCV)*, pages 12949–12958, 2021. 2

[23] Yifan Jiang, Peter Hedman, Ben Mildenhall, Dejia Xu, Jonathan T Barron, Zhangyang Wang, and Tianfan Xue. Alignerf: High-fidelity neural radiance fields via alignment-aware training. *IEEE/CVF Conference on Computer Vision and Pattern Recognition (CVPR)*, 2023. 2

[24] Kaizhang Kang, Zimin Chen, Jiaping Wang, Kun Zhou, and Hongzhi Wu. Efficient reflectance capture using an autoencoder. *ACM Transactions on Graphics (TOG)*, 37(4):127–1, 2018. 2

[25] Sosuke Kobayashi, Eiichi Matsumoto, and Vincent Sitzmann. Decomposing nerf for editing via feature field distillation. *Advances in Neural Information Processing Systems (NeurIPS)*, 2022. 2

[26] Edwin H Land and John J McCann. Lightness and retinex theory. *Journal of the Optical Society of America (1917-1983)*, 61(1):1, 1971. 3

[27] Yu Li and Michael S. Brown. Single image layer separation using relative smoothness. In *IEEE/CVF Conference on Computer Vision and Pattern Recognition (CVPR)*, 2014. 3

[28] Zhengqi Li and Noah Snavely. Cgintrinsics: Better intrinsic image decomposition through physically-based rendering. In *European Conference on Computer Vision (ECCV)*, pages 371–387, 2018. 3

[29] Zhengqi Li and Noah Snavely. Learning intrinsic image decomposition from watching the world. In *IEEE/CVF Conference on Computer Vision and Pattern Recognition (CVPR)*, pages 9039–9048, 2018. 3

[30] Zhengqin Li, Kalyan Sunkavalli, and Manmohan Chandraker. Materials for masses: Svbrdf acquisition with a single mobile phone image. In *European Conference on Computer Vision (ECCV)*, pages 72–87, 2018. 2

[31] Zhengqin Li, Zexiang Xu, Ravi Ramamoorthi, Kalyan Sunkavalli, and Manmohan Chandraker. Learning to reconstruct shape and spatially-varying reflectance from a single image. *ACM Transactions on Graphics (TOG)*, 37(6):1–11, 2018. 2

[32] Chen-Hsuan Lin, Jun Gao, Luming Tang, Towaki Takikawa, Xiaohui Zeng, Xun Huang, Karsten Kreis, Sanja Fidler, Ming-Yu Liu, and Tsung-Yi Lin. Magic3d: High-resolution text-to-3d content creation. *arXiv preprint arXiv:2211.10440*, 2022. 1

[33] Steven Liu, Xiuming Zhang, Zhoutong Zhang, Richard Zhang, Jun-Yan Zhu, and Bryan Russell. Editing conditional radiance fields. In *IEEE/CVF International Conference on Computer Vision (ICCV)*, 2021. 2

[34] Xinhang Liu, Jiaben Chen, Huai Yu, Yu-Wing Tai, and Chi-Keung Tang. Unsupervised multi-view object segmentation using radiance field propagation. *Advances in Neural Information Processing Systems (NeurIPS)*, 2022. 2

[35] Stephen Lombardi, Tomas Simon, Gabriel Schwartz, Michael Zollhoefer, Yaser Sheikh, and Jason Saragih. Mixture of volumetric primitives for efficient neural rendering. *ACM Transactions on Graphics (TOG)*, 40(4):1–13, 2021. 2

[36] Wojciech Matusik, Hanspeter Pfister, Matt Brand, and Leonard McMillan. A data-driven reflectance model. *ACM Transactions on Graphics (TOG)*, 22(3):759–769, 2003. 2

[37] Ben Mildenhall, Pratul P. Srinivasan, Matthew Tancik, Jonathan T. Barron, Ravi Ramamoorthi, and Ren Ng. Nerf: Representing scenes as neural radiance fields for view synthesis. In *European Conference on Computer Vision (ECCV)*, 2020. 1, 2, 3, 7

[38] Thomas Müller, Alex Evans, Christoph Schied, and Alexander Keller. Instant neural graphics primitives with a multiresolution hash encoding. *ACM Transactions on Graphics (TOG)*, 41(4):102:1–102:15, July 2022. 2

[39] Giljoo Nam, Joo Ho Lee, Diego Gutierrez, and Min H Kim. Practical svbrdf acquisition of 3d objects with unstructured flash photography. *ACM Transactions on Graphics (TOG)*, 37(6):1–12, 2018. 2

[40] Jannik Boll Nielsen, Henrik Wann Jensen, and Ravi Ramamoorthi. On optimal, minimal brdf sampling for reflectance acquisition. *ACM Transactions on Graphics (TOG)*, 34(6):1–11, 2015. 2

[41] Michael Niemeyer, Jonathan T. Barron, Ben Mildenhall, Mehdi S. M. Sajjadi, Andreas Geiger, and Noha Radwan. Regnerf: Regularizing neural radiance fields for view synthesis from sparse inputs. In *IEEE/CVF Conference on Computer Vision and Pattern Recognition (CVPR)*, 2022. 2

[42] Michael Oechsle, Songyou Peng, and Andreas Geiger. Unisurf: Unifying neural implicit surfaces and radiance fields for multi-view reconstruction. In *IEEE/CVF Conference on Computer Vision and Pattern Recognition (CVPR)*, pages 5589–5599, 2021. 2

[43] Keunhong Park, Utkarsh Sinha, Jonathan T. Barron, Sofien Bouaziz, Dan B Goldman, Steven M. Seitz, and Ricardo Martin-Brualla. Nerfies: Deformable neural radiance fields. *IEEE/CVF International Conference on Computer Vision (ICCV)*, 2021. 2

[44] Ben Poole, Ajay Jain, Jonathan T Barron, and Ben Mildenhall. Dreamfusion: Text-to-3d using 2d diffusion. *International Conference on Learning Representations (ICLR)*, 2023. 1

[45] Albert Pumarola, Enric Corona, Gerard Pons-Moll, and Francesc Moreno-Noguer. D-nerf: Neural radiance fields for dynamic scenes. In *IEEE/CVF Conference on Computer Vision and Pattern Recognition (CVPR)*, pages 10318–10327, 2021. 2

[46] Ravi Ramamoorthi and Pat Hanrahan. On the relationship between radiance and irradiance: determining the illumination from images of a convex lambertian object. *JOSA A*, 18(10):2448–2459, 2001. 4

[47] Konstantinos Rematas, Andrew Liu, Pratul P Srinivasan, Jonathan T Barron, Andrea Tagliasacchi, Thomas Funkhouser, and Vittorio Ferrari. Urban radiance fields. In *IEEE/CVF Conference on Computer Vision and Pattern Recognition (CVPR)*, pages 12932–12942, 2022. 1

[48] Zhongzheng Ren, Aseem Agarwala, Bryan Russell, Alexander G Schwing, and Oliver Wang. Neural volumetric object selection. In *IEEE/CVF Conference on Computer Vision and Pattern Recognition (CVPR)*, pages 6133–6142, 2022. 2, 8

[49] Mike Roberts, Jason Ramapuram, Anurag Ranjan, Atulit Kumar, Miguel Angel Bautista, Nathan Paczan, Russ Webb, and Joshua M Susskind. Hypersim: A photorealistic synthetic dataset for holistic indoor scene understanding. In *IEEE/CVF Conference on Computer Vision and Pattern Recognition (CVPR)*, pages 10912–10922, 2021. 6

[50] Carsten Rother, Martin Kiefel, Lumin Zhang, Bernhard Schölkopf, and Peter V Gehler. Recovering intrinsic images with a global sparsity prior on reflectance. In *Advances in Neural Information Processing Systems (NeurIPS)*, 2011. 3

[51] Johannes L Schonberger and Jan-Michael Frahm. Structure-from-motion revisited. In *IEEE/CVF Conference on Computer Vision and Pattern Recognition (CVPR)*, pages 4104–4113, 2016. 6

[52] Li Shen and Chuohao Yeo. Intrinsic images decomposition using a local and global sparse representation of reflectance.

In *IEEE/CVF Conference on Computer Vision and Pattern Recognition (CVPR)*, 2011. 3

[53] Peter-Pike Sloan, Jan Kautz, and John Snyder. Precomputed radiance transfer for real-time rendering in dynamic, low-frequency lighting environments. In *ACM Transactions on Graphics (SIGGRAPH)*, pages 527–536, 2002. 4

[54] Pratul P Srinivasan, Boyang Deng, Xiuming Zhang, Matthew Tancik, Ben Mildenhall, and Jonathan T Barron. Nerv: Neural reflectance and visibility fields for relighting and view synthesis. In *IEEE/CVF Conference on Computer Vision and Pattern Recognition (CVPR)*, pages 7495–7504, 2021. 3

[55] Matthew Tancik, Vincent Casser, Xinchen Yan, Sabeek Pradhan, Ben Mildenhall, Pratul P Srinivasan, Jonathan T Barron, and Henrik Kretzschmar. Block-nerf: Scalable large scene neural view synthesis. In *IEEE/CVF Conference on Computer Vision and Pattern Recognition (CVPR)*, pages 8248–8258, 2022. 1

[56] Edgar Tretschk, Ayush Tewari, Vladislav Golyanik, Michael Zollhöfer, Christoph Lassner, and Christian Theobalt. Non-rigid neural radiance fields: Reconstruction and novel view synthesis of a dynamic scene from monocular video. In *IEEE/CVF Conference on Computer Vision and Pattern Recognition (CVPR)*, pages 12959–12970, 2021. 2

[57] Dor Verbin, Peter Hedman, Ben Mildenhall, Todd Zickler, Jonathan T Barron, and Pratul P Srinivasan. Refnerf: Structured view-dependent appearance for neural radiance fields. In *IEEE/CVF Conference on Computer Vision and Pattern Recognition (CVPR)*, pages 5481–5490. IEEE, 2022. 3, 6

[58] Can Wang, Menglei Chai, Mingming He, Dongdong Chen, and Jing Liao. Clip-nerf: Text-and-image driven manipulation of neural radiance fields. In *IEEE/CVF Conference on Computer Vision and Pattern Recognition (CVPR)*, pages 3835–3844, 2022. 2

[59] Jiepeng Wang, Peng Wang, Xiaoxiao Long, Christian Theobalt, Taku Komura, Lingjie Liu, and Wenping Wang. Neuris: Neural reconstruction of indoor scenes using normal priors. In *European Conference on Computer Vision (ECCV)*, pages 139–155. Springer, 2022. 2

[60] Liao Wang, Jiakai Zhang, Xinhang Liu, Fuqiang Zhao, Yanshun Zhang, Yingliang Zhang, Minye Wu, Jingyi Yu, and Lan Xu. Fourier plenoctrees for dynamic radiance field rendering in real-time. In *IEEE/CVF Conference on Computer Vision and Pattern Recognition (CVPR)*, pages 13524–13534, 2022. 2

[61] Peng Wang, Lingjie Liu, Yuan Liu, Christian Theobalt, Taku Komura, and Wenping Wang. Neus: Learning neural implicit surfaces by volume rendering for multi-view reconstruction. *Advances in Neural Information Processing Systems (NeurIPS)*, 2021. 2

[62] Zhou Wang, Alan C Bovik, Hamid R Sheikh, and Eero P Simoncelli. Image quality assessment: from error visibility to structural similarity. *IEEE Transactions on Image Processing (TIP)*, 13(4):600–612, 2004. 7

[63] Yi Wei, Shaohui Liu, Yongming Rao, Wang Zhao, Jiwen Lu, and Jie Zhou. Nerfingmvs: Guided optimization of

neural radiance fields for indoor multi-view stereo. In *IEEE/CVF International Conference on Computer Vision (ICCV)*, pages 5610–5619, 2021. 2

[64] Xiuchao Wu, Jiamin Xu, Zihan Zhu, Hujun Bao, Qixing Huang, James Tompkin, and Weiwei Xu. Scalable neural indoor scene rendering. *ACM Transactions on Graphics (TOG)*, 41(4):1–16, 2022. 2

[65] Jiamin Xu, Xiuchao Wu, Zihan Zhu, Qixing Huang, Yin Yang, Hujun Bao, and Weiwei Xu. Scalable image-based indoor scene rendering with reflections. *ACM Transactions on Graphics (TOG)*, 40(4):1–14, 2021. 2

[66] Weicai Ye, Shuo Chen, Chong Bao, Hujun Bao, Marc Pollefeys, Zhaopeng Cui, and Guofeng Zhang. Intrinsicnerf: Learning intrinsic neural radiance fields for editable novel view synthesis. *arXiv preprint arXiv:2210.00647*, 2022. 3

[67] Alex Yu, Ruilong Li, Matthew Tancik, Hao Li, Ren Ng, and Angjoo Kanazawa. Plenoctrees for real-time rendering of neural radiance fields. In *IEEE/CVF International Conference on Computer Vision (ICCV)*, pages 5752–5761, 2021. 2

[68] Ye Yu and William AP Smith. Inverserendernet: Learning single image inverse rendering. In *IEEE/CVF Conference on Computer Vision and Pattern Recognition (CVPR)*, pages 3155–3164, 2019. 3

[69] Jiakai Zhang, Xinhang Liu, Xinyi Ye, Fuqiang Zhao, Yanshun Zhang, Minye Wu, Yingliang Zhang, Lan Xu, and Jingyi Yu. Editable free-viewpoint video using a layered neural representation. *ACM Transactions on Graphics (TOG)*, 40(4):1–18, 2021. 2

[70] Kai Zhang, Fujun Luan, Qianqian Wang, Kavita Bala, and Noah Snavely. Physg: Inverse rendering with spherical gaussians for physics-based material editing and relighting. In *IEEE/CVF Conference on Computer Vision and Pattern Recognition (CVPR)*, pages 5453–5462, 2021. 3

[71] Richard Zhang, Phillip Isola, Alexei A Efros, Eli Shechtman, and Oliver Wang. The unreasonable effectiveness of deep features as a perceptual metric. In *IEEE/CVF Conference on Computer Vision and Pattern Recognition (CVPR)*, pages 586–595, 2018. 7

[72] Fuqiang Zhao, Wei Yang, Jiakai Zhang, Pei Lin, Yingliang Zhang, Jingyi Yu, and Lan Xu. Humannerf: Efficiently generated human radiance field from sparse inputs. In *IEEE/CVF Conference on Computer Vision and Pattern Recognition (CVPR)*, pages 7743–7753, 2022. 1

[73] Shuaifeng Zhi, Tristan Laidlow, Stefan Leutenegger, and Andrew J Davison. In-place scene labelling and understanding with implicit scene representation. In *IEEE/CVF International Conference on Computer Vision (ICCV)*, pages 15838–15847, 2021. 2

[74] Rui Zhu, Zhengqin Li, Janarbek Matai, Fatih Porikli, and Manmohan Chandraker. Irisformer: Dense vision transformers for single-image inverse rendering in indoor scenes. In *IEEE/CVF Conference on Computer Vision and Pattern Recognition (CVPR)*, pages 2822–2831, 2022. 3